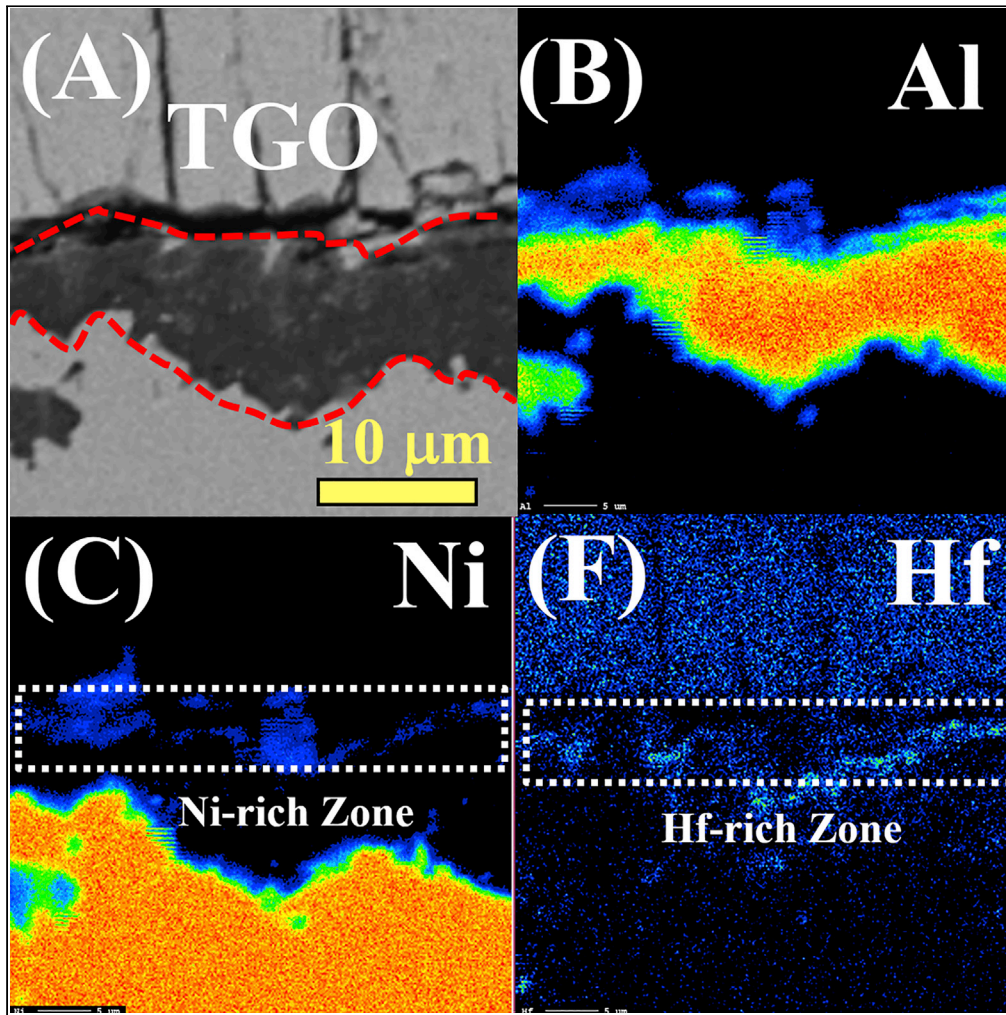CellPress

Article

Thermal property and failure behavior of LaSmZrO thermal barrier coatings by EB-PVD

Zaoyu Shen, Guanxi Liu, Rujing Zhang, Jianwei Dai, Limin He, Rende Mu

shenzaoyu@163.com (Z.S.)
murendeaecc@163.com (R.M.)

Highlights

The LaSmZrO ceramics show low thermal conductivity and high TEC

The LaSmZrO coatings show high thermal shock and cycling life at 1100°C

The LaSmZrO coatings might be regarded as one of the advanced thermal barrier coatings

Article

Thermal property and failure behavior of LaSmZrO thermal barrier coatings by EB-PVD

Zaoyu Shen,[1,2,*] Guanxi Liu,[1] Rujing Zhang,[1] Jianwei Dai,[1] Limin He,[1] and Rende Mu[1,*]

SUMMARY

$La_2Zr_2O_7$ coatings are promising candidates to substitute YSZ coatings in advanced gas turbine engines. In this work, Sm-doped $La_2Zr_2O_7$ coatings were deposited by physical vapor deposition. This work focuses on the crystal structure, thermal conductivity, thermal expansion coefficient, morphology, composition, and thermal durability of LaSmZrO coatings. The LaSmZrO ceramics exhibit low thermal conductivity (1.69 W/mK at 800°C) and high thermal expansion coefficient ($9.72*10^{-6}$ K^{-1} at 1500°C) compared with $La_2Zr_2O_7$. The LaSmZrO/YSZ coatings with feathery microstructure show relatively good thermal durability (8183 cycles or 856 h) under high temperature. The broken regions are observed at the ceramic coating/bond coating interface. The failure behaviors are relevant with crack evolution and thermally grown oxide growth. This work might guide the investigation of advanced coatings under high temperature.

INTRODUCTION

Advanced gas turbines have been widely used as power sources for aircrafts. During service, hot components of gas turbines need to face complex and harsh conditions (oxidation, erosion, and corrosion) under high temperatures (Padture et al., 2002; Clarke et al., 2012; Levi, 2002; Vaßen et al., 2010; Sampath et al., 2012). Thus, the demand for advanced gas turbines needs to grow along with the development of related aviation technology. Among them, thermal barrier coatings (TBCs) have a significant effect on the development of next-generation gas turbine engines. As we know, TBCs would provide effective protection for hot components of gas turbines during service because of their thermal conductivity, thermal stability, and thermal expansion coefficient. Nowadays, the main deposition technology of TBCs include atmospheric plasma spraying, electron beam-physical vapor deposition (EB-PVD), suspension plasma spray, and plasma spray-physical vapor deposition (Vaßen et al., 2010; Sampath et al., 2012; Pollock et al., 2012; Karaoglanli et al., 2020a, 2020b; Kaplan et al., 2019). Among them, EB-PVD technology is a sophisticated TBCs deposition technology for rotating parts of advanced gas turbins (Padture et al., 2002; Clarke et al., 2012). At present, TBCs are metallic coating + ceramic coating complex systems. The Y doping ZrO_2 (YSZ) has been applied in gas turbine as TBCs. However, YSZ usually exhibits poor thermal durability owing to the phase instability and low sintering resistance above 1200°C (Vaßen et al., 2010; Sampath et al., 2012).

To improve the thermal durability, researchers and institutions have explored novel ceramic materials. The novel ceramics ($La_2Zr_2O_7$, $Gd_2Zr_2O_7$ and Re-ZrO_2) have been studied to substitute YSZ because of their good thermal property (Pollock et al., 2012; Karaoglanli et al., 2020a, 2020b; Kaplan et al., 2019; Zhao et al., 2017; Zhang et al., 2015, 2020; Shen et al., 2018, 2019, 2021a, 2021b, 2021c; Mahade et al., 2017; Gok and Goller, 2016; Shen et al., 2021a, 2021b, 2021c; Hong et al., 2015; Ozgurluk et al., 2021a, 2021b; Zhou et al., 2017, 2020, 2021; Ozgurluk et al., 2018, 2021a, 2021b; Doleker et al., 2020). Among advance ceramics, $La_2Zr_2O_7$ (LZ) has been widely studied owing to its relatively low thermal conductivity, high melting point, and thermal stability compared with YSZ (Vaßen et al., 2010; Sampath et al., 2012). To further reduce thermal conductivity, the heavy atomic mass and complex atomic structure of rare elements (Ce, Yb, Y, and Gd) have been chosen to substitute in A site or B site of LZ ceramics (Vaßen et al., 2010; Sampath et al., 2012; Zhou et al., 2019; Shen et al., 2020; Wang et al., 2015; Wan et al., 2009; Bahamirian et al., 2019; Song et al., 2020). The doping element might produce many point defects into the $La_2Zr_2O_7$ crystal, which can improve the phonon-point defect scattering, leading to the reduction of thermal conductivity. On the other hand, the LZ, doped by rare elements with heavy atomic mass and complex atomic structure, exhibits a high thermal property in comparison to YSZ (Vaßen et al., 2010; Sampath et al., 2012). The high
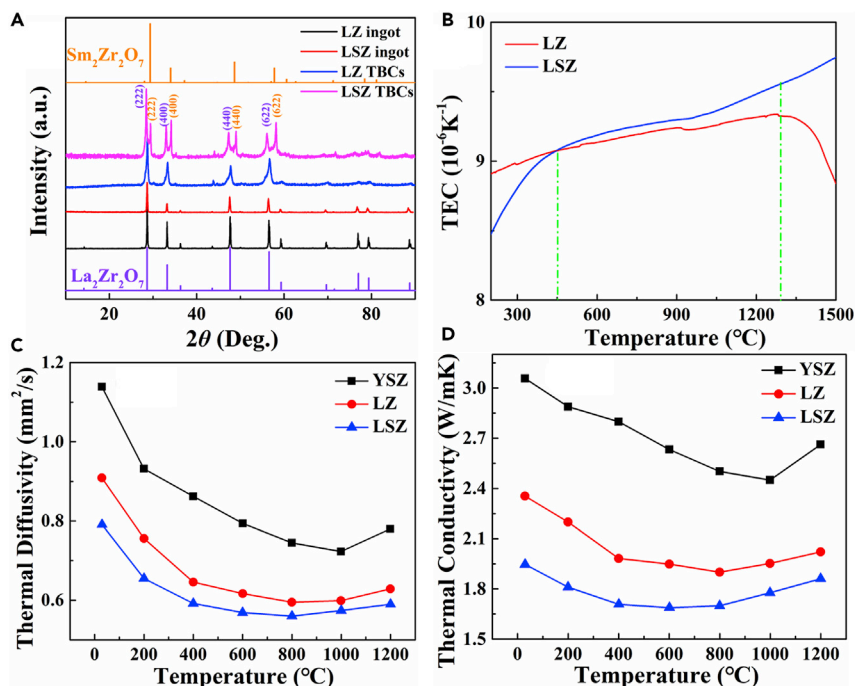
Figure 1. The crystal structure, thermal expansion coefficient, thermal diffusivity, and thermal conductivity of coatings and ceramics
(A) XRD patterns of LZ, LSZ, ingot and TBCs, (B) thermal expansion coefficient of LZ and LSZ ceramics, (C) thermal diffusivity, and (D) thermal conductivity of the YSZ, LZ, and LSZ ceramics.

thermal expansion coefficient and phase stability of advanced TBCs can alleviate residual stress and improve thermal protection ability leading to high thermal cycling life. However, seldom work systematically focuses on the La site substitution of LZ ceramics and their TBCs by EB-PVD. To further improve thermal property, the Sm element was selected to partially substitute for La site of $La_2Zr_2O_7$. The effect of Sm substitution on the structure, property, and thermal durability has yet to be studied in the literature. Furthermore, the relationship between cracks evolution and thermally grown oxide (TGO) growth still remains to be a challenge in the study of TBCs failure.

The objective of the work is to study the LaSmZrO (LSZ) as advanced TBCs. The LaSmZrO coatings were prepared by electron beam-physical vapor deposition. The phase, composition, and microstructure of LaSmZrO coatings were investigated by XRD, SEM, EDS, EPMA, and TEM. The relationship between cracks evolution and interface stability has been investigated in this work.

RESULTS AND DISCUSSION

Crystal structure

The XRD results obtained from LZ ingot, LSZ ingot, LZ as-deposited TBCs, and LSZ as-deposited TBCs are shown in Figure 1A. The XRD patterns of LZ ingot and LSZ ingot exhibit a relatively pure cubic pyrochlore type crystal structure (No. 17-0450). The diffraction peak of LZ and LSZ ingots at 28.66°, 33.23°, 47.56°, and 56.41° belong to (222), (400), (440), and (622) of $La_2Zr_2O_7$ phases. It indicates that the solid solution structure of LaSmZrO ingot is formed in a solid state reaction because of the similar ionic radius of Sm^{3+} (1.08 Å) and La^{3+} (1.16 Å). After deposition, XRD of LZ TBCs exhibits a pure cubic pyrochlore type crystal structure corresponding to $La_2Zr_2O_7$ phases. The XRD of as-deposited LSZ TBCs exhibit a composited crystal structure. The peaks at 28.46°, 33.02°, 47.31°, and 56.04° belong to (222), (400), (440), and (622) of $La_2Zr_2O_7$ phases. The peaks at 29.42°, 34.14°, 49.00°, and 58.10° belong to (222), (400), (440), and (622) of $Sm_2Zr_2O_7$ phases. It indicates that a composite of $La_2Zr_2O_7$ and $Sm_2Zr_2O_7$ has been formed after the EB-PVD process. In addition, the LZ as-deposited TBCs and LSZ as-deposited TBCs show the broad and low diffraction peaks corresponding to the existence of hierarchical structures.

Thermal conductivity

In the field of TBCs, low thermal conductivity is the key property dominating the heat insulation ability to substrate (Sampath et al., 2012). The thermal diffusivity of YSZ, LZ, and LSZ ceramics were detected by Netzsch LFA 427. The value of thermal conductivity of YSZ, LZ, and LSZ ceramics were calculated by the formula ($\lambda = \rho \times \alpha \times Cp$) (Zhao et al., 2017; Kubaschewski et al., 1993). The thermal diffusivity and thermal conductivity of all ceramics exhibit a tendency to decrease first and then increase in the range of 30°C–1500°C (Figures 1C and 1D). The minimum value of YSZ ceramics is about 2.45 W/mK at 1000°C. The minimum value of LSZ ceramics is about 1.69 W/mK at 800°C, whereas the minimum value of LZ ceramics is about 1.90 W/mK at 800°C. The minimum value of thermal conductivity of LSZ ceramics is about 30% lower than YSZ ceramics and about 11% lower than LZ ceramics.

In general, the complexity of crystal structure has an important effect on the reduction of thermal conductivity because of the increasing number of optical phonons. Furthermore, increasing the number of optical states also increases the number of available phonon-phonon interactions leading to the reduction of thermal conductivity (Zhao et al., 2017; Kubaschewski et al., 1993).[] According to XRD analysis, the Sm^{3+} substitutes for La^{3+} site of $La_2Zr_2O_7$ leading to a composite of $La_2Zr_2O_7$ and $Sm_2Zr_2O_7$ crystals. Owing to the mass and ionic radius difference between Sm^{3+} (1.08 Å) and La^{3+} (1.16 Å), a lot of point defects would be introduced in $La_2Zr_2O_7$ material. The substitution of La^{3+} by Sm^{3+} might introduce strain fluctuations, leading to the relatively high heat-carrying phonons. Thus, the Sm rare earth doping in $La_2Zr_2O_7$ would lead to the effective reduction of thermal conductivity. In DCL TBCs systems, the reduction of thermal conductivity has an important effect on the thermal cycling life of TBCs under high temperature. In the cooling-heating process, the LSZ coating with low thermal conductivity might provide the thermal gradient condition, leading to good thermal protection and high thermal cycling life.

Thermal expansion coefficient

Although thermal conductivity of ceramics is the key metric for advanced ceramic materials, it is also essential that thermal expansion coefficient (TEC) is another key metric for thermomechanical compatibility with bond coating and the intermediate ceramic coating (Pan et al., 2012; Li et al., 2020; Wu et al., 2019). As we know, the TEC mismatch among the substrate, bond coating, and ceramic coating would lead to high thermal stresses in TBCs system that might further promote the TBCs failure. Thus, the high TEC of ceramics would have a significant role on the thermal property. TEC results that were obtained from LZ ceramics and LSZ ceramics are shown in Figure 1B. At low temperature, the TEC value of LSZ ceramics is relatively lower than LZ ceramics below 450°C. The TEC value of LSZ ceramics is relatively higher compared with LZ ceramics above 450°C. TEC value of LSZ ceramics is 9.72×10^{-6} K^{-1} at 1500°C, which is about 10% higher than LZ ceramics. In addition, the TEC curve of LZ decreases above 1300°C owing to the sintering effect of LZ ceramics. It indicates that LSZ ceramics would have a better sintering temperature which is about 200°C higher than LZ ceramics. In general, ionic radius/cationic field strength on the introduction of Sm^{3+} (1.08 Å) has a significant effect on the improvement of TEC of $La_2Zr_2O_7$. In addition, the substitution of Sm^{3+} for La^{3+} can produce point defects in $La_2Zr_2O_7$, which would further introduce a stress field and enhance the anharmonic vibration in the lattice leading to the improvement of TEC (Zhao et al., 2017). In the DCL-TBCs system, the improvement of TEC plays an important role on the thermal cycling life of TBCs under high temperature. In the cooling-heating process, the high TEC of LSZ coating would provide the high thermomechanical compatibility to bond coating and substrate compared with LZ coating, thus leading to high thermal cycling life (Zhao et al., 2017).

Morphology and composition

Figure 2A shows typical cross-section morphology of as-deposited LaSmZrO coatings. It clearly shows that the TBCs system consisted of a bond coating with a thickness of about 30-40 μm, a middle ceramic coating with a thickness of about 70-80 μm, and a top ceramic coating with a thickness of about 70-80 μm. The thickness ratio of top ceramic coating: middle ceramic coating: bond coating is about 1.0:1.0:0.5. Further investigation indicates that the morphology of middle and top ceramic coating is a columnar structure, whereas the morphology of the bond coating is a typical equiaxed structure. The three-coating system exhibits smooth and good bonding because of the AIP-PVD and EB-PVD process.

As shown in Figure 2B, EDS line scanning has been detected in cross-section of TBCs. The Ni, Co, Cr, Al, Y, and Hf elements mainly exist in the bond coating corresponding to the NiCoCrAlYHf. The La, Sm, Zr, and O elements mainly exist in the layer corresponding to the LaSmZrO. The Zr and O elements mainly exist in the
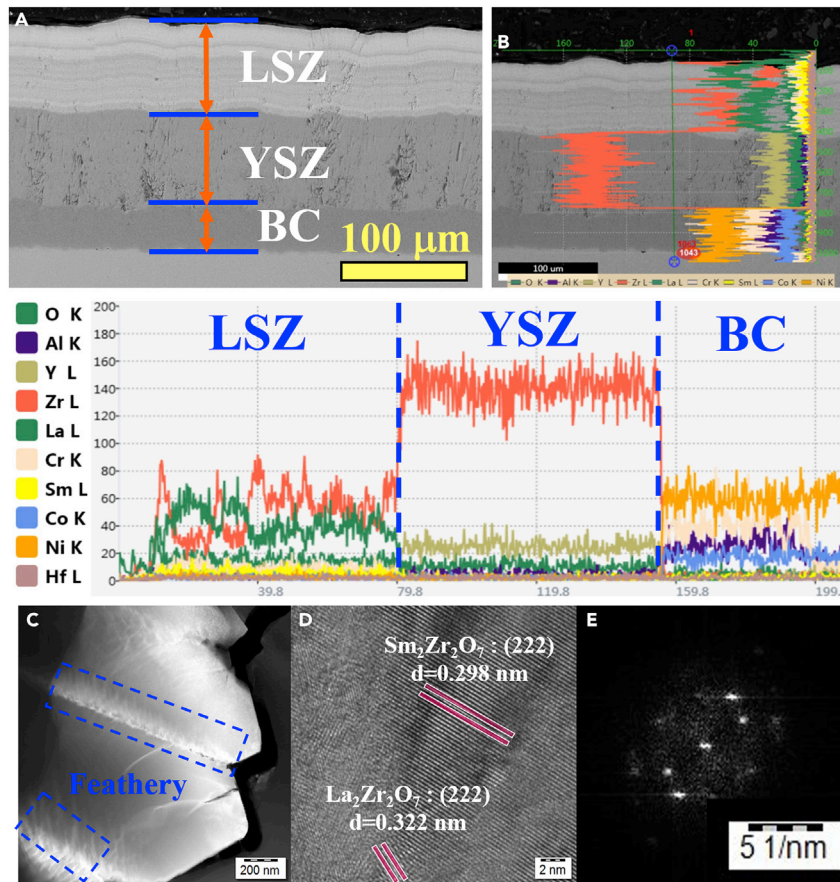
Figure 2. The morphology and composition of TBCs
(A) Cross-section morphology, (B) EDS line scanning, (C) HAADF image, (D) HRTEM image, and (E) FFT pattern of the LSZ.

middle layer corresponding to the YSZ. The content distribution of the Zr element clearly confirms three layers of coating structure.

As shown in Figures 2C–2E, the microstructure of LSZ coating was further investigated by TEM. As shown in Figure 2C, the LSZ coating exhibits a feathery microstructure at columnar gaps. The HRTEM is carried out on the thin area of the LSZ coating (Figure 2D). Further investigation indicates that the interplanar Spacing (d) of LSZ is 0.322 nm belonging to the (222) plane of $La_2Zr_2O_7$, whereas the interplanar Spacing (d) of LSZ is 0.298 nm belonging to the (222) plane of $Sm_2Zr_2O_7$. In addition, the corresponding Fast Fourier Transform (FFT) pattern of LSZ demonstrates the composited crystal structure of $La_2Zr_2O_7$ and $Sm_2Zr_2O_7$ (Figure 2E).

To further analyze the element distribution of LSZ + YSZ + NiCoCrAlYHf TBCs system, the cross-section morphology was detected by using EPMA technology. As shown in Figure 3, the EPMA images provide a visualization of morphology and composition of LSZ/YSZ DCL TBCs. The La, Sm, and O elements mainly exist in top ceramic coating corresponding to the LaSmZrO coating. The Cr, Co, Al, Y, and Hf elements mainly exist in bond coating corresponding to the NiCoCrAlYHf coating. As shown in Figures 3B and 3C, the La and Sm elements are distributed homogeneously throughout the LSZ coating. Further investigation indicates that the difference of Y element concentration also indicates the formation of the three-coating structure.

Thermal durability

Owing to the low thermal conductivity and high TEC, the LSZ ceramics might be used as an advanced TBCs material to provide thermal insulation in advanced aeroengines. As shown in Figures 4A and 4B, the
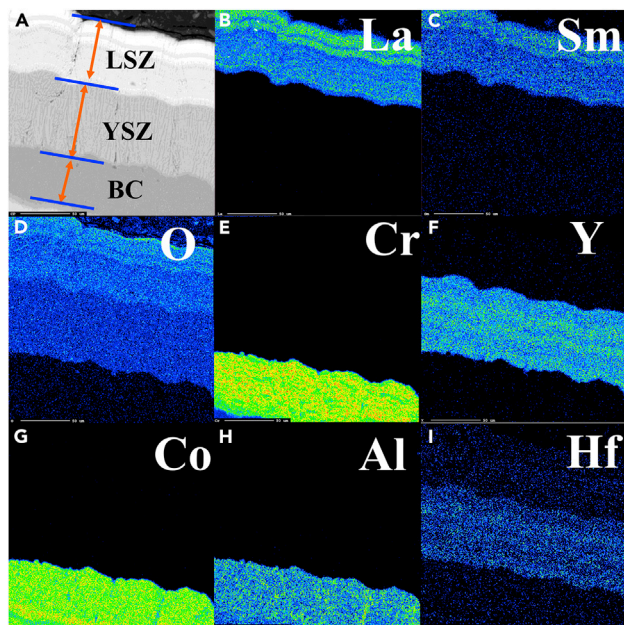
Figure 3. EPMA images of the as-deposited LSZ/YSZ TBCs
(A) Cross-section morphology, (B) La, (C) Sm, (D) O, (E) Cr, (F) Y, (G) Co, (H) Al, and (I) Hf.

thermal shock life and thermal cycling life of LSZ/YSZ DCL TBCs and LSZ single TBCs were detected at 1100°C. The average thermal shock life of LSZ/YSZ is about 8183 cycles, whereas the average thermal shock life of LSZ is only about 273 cycles. The thermal shock life of LSZ/YSZ is about 30 times higher than that of LSZ. In addition, the average thermal cycling life of LSZ/YSZ is about 856 h, which is about 18 times higher than that of LSZ (48 h thermal cycling life). The LSZ/YSZ DCL TBCs exhibits a high thermal durability compared with other advanced coatings (Vaßen et al., 2010; Zhang et al., 2020; Shen et al., 2021a, 2021b, 2021c; Mahade et al., 2017; Wan et al., 2009; Bahamirian et al., 2019; Song et al., 2020).

According to the crystal structure, thermal conductivity, thermal expansion coefficient, morphology, and composition data, the reasons for the high thermal durability of LSZ/YSZ DCL TBCs could be summarized as the following aspects. Firstly, the Sm substitution in La site of $La_2Zr_2O_7$ leads to a dual phase structure of $La_2Zr_2O_7$ and $Sm_2Zr_2O_7$. The dual phase structure of TBCs would introduce many point defects and the relatively complex phonon scattering leading to the low thermal conductivity. The low thermal conductivity would introduce high thermal gradient condition in the cooling-heating process. The thermal gradient condition between ceramic coating and substrate would produce good heat insulation leading to the thermal durability extension of TBCs (Dong et al., 2020; Shen et al., 2021a, 2021b, 2021c). Secondly, the LaSmZrO/YSZ TBCs introduce the relatively complex defects leading to stress field and enhance the anharmonic vibration that would lead to the improvement of TEC. The high value of TEC would produce good thermomechanical protection to bond coating and further to substrate that might lead to the thermal durability extension of TBCs. Thirdly, the feathery morphology of TBCs provide a high level of strain tolerance and pseudoplasticity. In the cooling-heating process, the feathery morphology would alleviate residual stress in TBCs system leading to the thermal durability extension of TBCs (Padture et al., 2002; Clarke et al., 2012). In addition, the Sm substitution in La site of $La_2Zr_2O_7$ also introduces the relatively complex thermodynamically immobile defect clusters, which would improve the sintering resistance leading to the thermal durability extension of TBCs (Karaoglanli et al., 2020a, 2020b). On the whole, the reduction of thermal conductivity, the improvement of thermal expansion coefficient, and the feathery morphology of TBCs result in the thermal durability extension of LSZ/YSZ TBCs.

Failure behaviors

The failure behaviors of LSZ/YSZ DCL TBCs are systematically investigated after the thermal durability test. The cross-section morphology of ceramic coating (LSZ + YSZ), thermally grown oxide layer, and
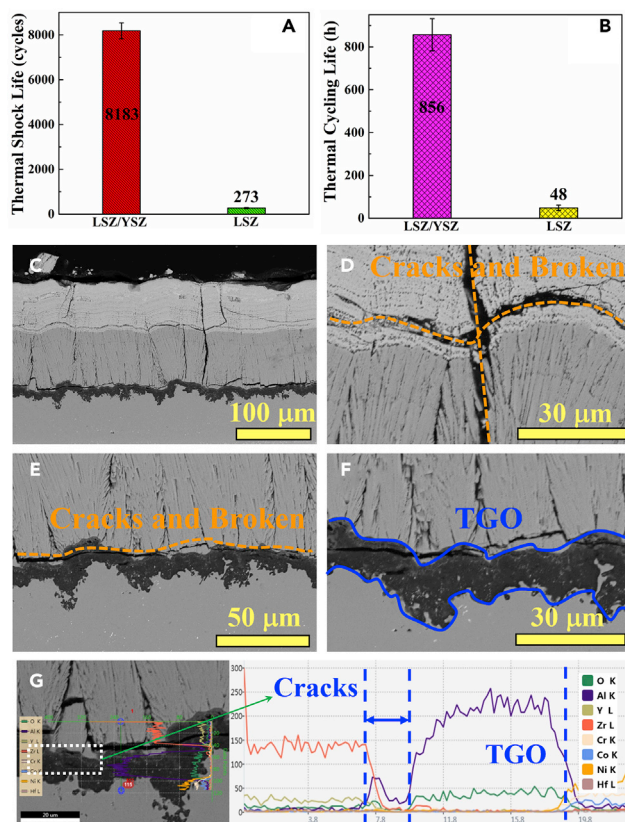
Figure 4. Thermal durability and morphology evolution of LSZ/YSZ TBCs
(A) The thermal shock life, (B) thermal cycling life, (C) cross-section morphology of TBCs, (D) DCL interface, (E) YSZ/BC interface, (F) TGO interface, and (G) EDS line scanning after thermal durability test.

NiCoCrAlYHf bond coating is shown in Figure 4. In TBCs system, the LSZ and YSZ coating still exhibit the columnar structure, whereas the bond coating still exhibits the equiaxed structure. The LSZ + YSZ + NiCoCrAlYHf system exhibits relatively good thermal stability under 1100°C. The LSZ/YSZ interface occurs after a delamination interface after thermal cycling test. As shown in Figure 4D, the horizontal and vertical cracks are mainly detected LSZ/YSZ interface owing to the different TEC's between LSZ ($9.72*10^{-6}$ K^{-1}) and YSZ (about $11*10^{-6}$ K^{-1}). As shown in Figure 4E, a lot of horizontal cracks coalesce into a broken line leading to the damage of YSZ columnar above TGO (about 5 μm). With the cooling-heating process, the broken regions caused by the crack evolution have spread over the interface between YSZ and TGO, leading to the failure of TBCs system (Liu et al., 2015; Jonnalagadda et al., 2017; Chen et al., 2018; Parlakyigit et al., 2020; Karaoglanli et al., 2020a, 2020b; Doleker et al., 2021a, 2021b, 2021b). As shown in Figure 4F, the thickness of TGO is about 10 μm after thermal durability test.

As shown in Figure 4G, the element distribution of YSZ/TGO/BC interface has been investigated by using EDS-line scanning. The existence of Al and O reveal relatively uniform distribution in TGO (mainly Al$_2$O$_3$). The peak of the purple line is the position of Al$_2$O$_3$, whereas the valley of the purple line is the position of horizontal crack. Further investigation also indicates that the thickness of TGO is about 10 μm after the thermal cycling test. To further elucidate the element evolution and failure behaviors of TBCs systems, TGO morphology and EPMA images of LSZ/YSZ TBCs were investigated after thermal durability test. As shown in Figure 5A, the TGO was formed between YSZ and bond coating with the cooling-heating process. Some bright zones were formed in TGO after thermal cycling life. Figures 5B–5F show the element distribution in TGO corresponding to the Al, Ni, Co, Cr, and Hf five elements. As shown in Figure 5B, the Al element is mainly concentrated in the TGO. As shown in Figures 5C–5E, the Ni, Co, and Cr element are mainly concentrated in the bond coating (Figure 5B). Further investigation indicates that the Ni, Co, and Cr three elements have diffused from NiCoCrAlYHf bond coating to TGO layer leading to the formation of Ni-Co-Cr-rich zone. In addition, the Hf element is also partly diffused and concentrated in the TGO layer
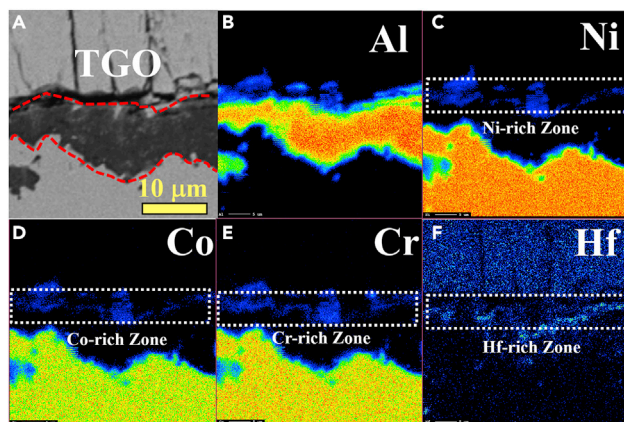
Figure 5. EPMA images of the LSZ/YSZ TBCs after thermal durability test
(A) Cross-section morphology of TGO, EPMA mapping images: (B) Al, (C) Ni, (D) Co, (E) Cr, and (F) Hf after thermal durability test.

leading to the formation of the Hf-rich zone. Further investigation indicates that the position of Ni, Co, Cr, and Hf element rich zones is almost the same in the TGO layer. That is to say, the diffusion of Al, Ni, Co, Cr, and Hf would lead to the formation of Ni-Al-Cr-Co-Hf oxides (Doleker et al., 2021a, 2021b, 2021a, 2021b; Chen et al., 2017; Yang et al., 2017; Shen et al., 2022; Doleker et al., 2019a, 2019b; Ozgurluk et al., 2019a, 2019b). These TEC mismatches between Ni-Al-Cr-Co-Hf oxides and Al_2O_3 might lead to the formation and growth of interface instability. The element diffusion in TBCs system would bring some volume change in the cooling-heating process. The volume change would lead to the growth of residual stresses and the crack evolution(Doleker et al., 2019a, 2019b; Evans et al., 2001, 2008; Ghadami et al., 2021; Balint et al., 2011). As a result, the element diffusion might be a critical factor for cracks' extension leading to the failure of TBCs. The investigation on failure behaviors will provide some insights on the effect of element and crack evolution on the failure of other TBCs systems.

Conclusions

The LaSmZrO/YSZ coatings are deposited by EB-PVD. The LaSmZrO coating mainly exhibits composite crystal structure. The coatings are composed of LaSmZrO, YSZ, and NiCoCrAlYHf coatings. The LaSmZrO coating exhibits a relatively high thermal durability because of the reduction of thermal conductivity, the improvement of TEC, the doping effect of Sm, and the feathery microstructure. The crack evolution and TGO growth lead to the instability of the TBCs system and play a key role in the failure mechanism of TBCs. The LaSmZrO coating might be one of the advanced TBCs materials.

Limitations of the study

The analysis given by furnace cycle tests is not detailed, because there was a temperature gradient between the ceramic coatings and bond coatings in the service. Thus, thermal durability requires follow-up experiments and in-depth investigation.

STAR★METHODS

Detailed methods are provided in the online version of this paper and include the following:

- KEY RESOURCES TABLE
- RESOURCE AVAILABILITY
  - Lead contact
  - Materials availability
  - Data and code availability
- EXPERIMENTAL MODEL AND SUBJECT DETAILS
- METHOD DETAILS
  - Preparation of TBCs
  - Characterizations
  - Furnace cycle tests

AUTHOR CONTRIBUTIONS

Conceptualization, Z.Y.S.; Funding, Z.Y.S.; Writing – Original Draft, Z.Y.S.; Data Curation, G.X.L. and R.D.M.; Formal Analysis, G.X.L.; Writing, R.J.Z.; Investigation, J.W.D. and L.M.H.; Resources, L.M.H. and R.D.M.

DECLARATION OF INTERESTS

The authors declare no competing interests.

REFERENCES

Bahamirian, M., Hadavi, S.M.M., Farvizi, M., Rahimipour, M.R., and Keyvani, A. (2019). Phase stability of ZrO_2 9.5Y_2O_3 5.6Yb_2O_3 5.2Gd_2O_3 compound at 1100°C and 1300°C for advanced TBC applications. Ceram. Int. 45, 7344–7350.

Balint, D.S., Kim, S.S., Liu, Y.F., Kitazawa, R., Kagawa, Y., and Evans, A.G. (2011). Anisotropic TGO rumpling in EB-PVD thermal barrier coatings under in-phase thermomechanical loading. Acta Mater. 59, 2544–2555.

Chen, Y., Zhao, X., Bai, M., Yang, L., Li, C., Wang, L., Carr, J.A., and Xiao, P. (2017). A mechanistic understanding on rumpling of a NiCoCrAlY bond coat for thermal barrier coating applications. Acta Mater. 128, 31–42.

Chen, Y., Zhao, X.F., and Xiao, P. (2018). Effect of microstructure on early oxidation of MCrAlY coatings. Acta Mater. 159, 150–162.

Clarke, D.R., Oechsner, M., and Padture, N.P. (2012). Thermal-barrier coatings for more efficient gas-turbine engines. MRS Bull 37, 891–898.

Doleker, K.M., Ozgurluk, Y., Ahlatci, H., and Karaoglanli, A.C. (2019a). Evaluation of oxidation and thermal cyclic behavior of YSZ, $Gd_2Zr_2O_7$ and YSZ/$Gd_2Zr_2O_7$ TBCs. Surf. Coat. Technol. 371, 262–275.

Doleker, K.M., Odabas, O., Ozgurluk, Y., Askerov, H., and Karaoglanli, A.C. (2019b). Effect of high temperature oxidation on Inconel 718 and Inconel 718/YSZ/$Gd_2Zr_2O_7$. Mater. Res. Express 6, 086456.

Doleker, K.M., Karaoglanli, A.C., Ozgurluk, Y., and Kobayashi, A. (2020). Performance of single YSZ, $Gd_2Zr_2O_7$ and double-layered YSZ/$Gd_2Zr_2O_7$ thermal barrier coatings in isothermal oxidation test conditions. Vacuum 177, 109401.

Doleker, K.M., Ozgurluk, Y., Kahraman, Y., and Karaoglanli, A.C. (2021a). Oxidation and hot corrosion resistance of HVOF/EB-PVD thermal barrier coating system. Surf. Coat. Technol. 409, 126862.

Doleker, K.M., Ozgurluk, Y., and Karaoglanli, A.C. (2021b). TGO growth and kinetic study of single and double layered TBC systems. Surf. Coat. Technol. 415, 127135.

Dong, S.J., Zhang, F.N., Li, N., Zeng, J.Y., Liang, P.P., Zhang, H., Liao, H.Q., Jiang, J.N., Deng, L.H., and Cao, X.Q. (2020). Thermal radiation and cycling properties of (Ca, Fe) or (Sr, Mn) co-doped $La_2Ce_2O_7$ coatings. J. Eur. Ceram. Soc. 40, 2020–2029.

Evans, A.G., Mumm, D.R., Hutchinson, J.W., Meier, G.H., and Pettit, F.S. (2001). Mechanisms controlling the curability of thermal barrier coatings. Prog. Mater. Sci. 46, 505–553.

Evans, A.G., Clarke, D.R., and Levi, C.G. (2008). The influence of oxides on the performance of advanced gas turbines. J. Eur. Ceram. Soc. 28, 1405–1419.

Ghadami, F., Aghdam, A.S.R., and Ghadami, S. (2021). Microstructural characteristics and oxidation behavior of the modified MCrAlX coatings: a critical review. Vacuum 185, 109980.

Gok, M.G., and Goller, G. (2016). Production and characterization of GZ/CYSZ alternative thermal barrier coatings with multilayered and functionally graded designs. J. Eur. Ceram. Soc. 36, 1755–1764.

Hong, Q.J., Ushakov, S.V., Navrotsky, A., and Walle, A. (2015). Combined computational and experimental investigation of the refractory properties of $La_2Zr_2O_7$. Acta Mater. 84, 275–282.

Jonnalagadda, K.P., Eriksson, R., Yuan, K., Li, X.H., Ji, X.J., Yu, Y.G., and Peng, R.L. (2017). A study of damage evolution in high purity nano TBCs during thermal cycling: a fracture mechanics based modelling approach. J. Eur. Ceram. Soc. 37, 2889–2899.

Kaplan, M., Uyaner, M., Ozgurluk, Y., Doleker, K.M., and Karaoglanli, A.C. (2019). Evaluation of hot corrosion behavior of APS and HVOF sprayed thermal barrier coatings (TBCs) exposed to molten $Na_2SO_4 + V_2O_5$ salt at 1000°C. In Engineering Design Applications, vol 92, A. Öchsner and H. Altenbach, eds. Advanced Structured Materials (Springer).

Karaoglanli, A.C., Ozgurluk, Y., and Doleker, K.M. (2020a). Comparison of microstructure and oxidation behavior of CoNiCrAlY coatings produced by APS, SSAPS, D-gun, HVOF and CGDS techniques. Vacuum 180, 109609.

Karaoglanli, A.C., Doleker, K.M., and Ozgurluk, Y. (2020b). Interface failure behavior of yttria stabilized zirconia (YSZ), $La_2Zr_2O_7$, $Gd_2Zr_2O_7$, YSZ/$La_2Zr_2O_7$ and YSZ/$Gd_2Zr_2O_7$ thermal barrier coatings (TBCs) in thermal cyclic exposure. Mater. Charact. 159, 110072.

Kubaschewski, O., Alock, C.B., and Spencer, P.J. (1993). Materials Thermochemistry, 6th edn. (Pergamon Press), p. 254.

Levi, C.G. (2002). Emerging materials and processes for thermal barrier systems. Curr. Opin. Solid State Mater. Sci. 8, 77–91.

Li, Y.R., Wang, J.M., and Wang, J.Y. (2020). Theoretical investigation of phonon contributions to thermal expansion coefficients for rare earth monosilicates RE_2SiO_5 (RE = Dy, Ho, Er, Tm, Yb and Lu). J. Eur. Ceram. Soc. 40, 2658–2666.

Liu, D., Rinaldi, C., and Flewitt, P.E.J. (2015). Effect of substrate curvature on the evolution of microstructure and residual stresses in EBPVD-TBC. J. Eur. Ceram. Soc. 35, 2563–2575.

Mahade, S., Curry, N., Björklund, S., Markocsan, N., Nylén, P., and Vaßen, R. (2017). Functional

performance of Gd$_2$Zr$_2$O$_7$/YSZ multi-layered thermal barrier coatings deposited by suspension plasma spray. Surf. Coat. Technol. *318*, 208–216.

Ozgurluk, Y., Doleker, K.M., and Karaoglanli, A.C. (2018). Hot corrosion behavior of YSZ, Gd$_2$Zr$_2$O$_7$ and YSZ/Gd$_2$Zr$_2$O$_7$ thermal barrier coatings exposed to molten sulfate and vanadate salt. Appl. Surf. Sci. *438*, 96–113.

Ozgurluk, Y., Doleker, K.M., and Karaoglanli, A.C. (2019a). Investigation of the effect of V$_2$O$_5$ and Na$_2$SO$_4$ melted salts on thermal barrier coatings under cyclic conditions. Anti-corros. Method. M. *66*, 644–650.

Ozgurluk, Y., Doleker, K.M., Ozkan, D., Ahlatci, H., and Karaoglanli, A.C. (2019b). Cyclic hot corrosion failure behaviors of EB-PVD TBC systems in the presence of sulfate and vanadate molten salts. Coatings *9*, 166.

Ozgurluk, Y., Doleker, K.M., Ahlatci, H., and Karaoglanli, A.C. (2021a). Investigation of calcium-magnesium-alumino-silicate (CMAS) resistance and hot corrosion behavior of YSZ and La$_2$Zr$_2$O$_7$/YSZ thermal barrier coatings (TBCs) produced with CGDS method. Surf. Coat. Technol. *411*, 126969.

Ozgurluk, Y., Karaoglanli, A.C., and Ahlatci, H. (2021b). Comparison of calcium-magnesium-alumina-silicate (CMAS) resistance behavior of produced with electron beam physical vapor deposition (EB-PVD) method YSZ and Gd$_2$Zr$_2$O$_7$/YSZ thermal barrier coatings systems. Vacuum *194*, 110576.

Padture, N.P., Gell, M., and Jordan, E.H. (2002). Thermal barrier coatings for gas-turbine engine applications. Science *296*, 280–284.

Pan, W., Phillpot, S.R., Wan, C.L., Chernatynskiy, A., and Qu, Z.X. (2012). Low thermal conductivity oxides. MRS Bull *37*, 917–922.

Parlakyigit, A.S., Ozkan, D., Oge, M., Ozgurluk, Y., Doleker, K.M., Gulmez, T., and Karaoglanli, A.C. (2020). Formation and growth behavior of TGO layer in TBCs with HVOF sprayed NiCr bond coat. Emerg. Mater. Res. *9*, 451–459.

Pollock, T.M., Lipkin, D.M., and Hemker, K.J. (2012). Multifunctional coating interlayers for thermal-barrier systems. MRS Bull *37*, 923–931.

Sampath, S., Schulz, U., Jarligo, M.O., and Kuroda, S. (2012). Processing science of advanced thermal-barrier systems. MRS Bull *37*, 903–910.

Shen, Z.Y., He, L.M., Xu, Z.H., Mu, R.D., and Huang, G.H. (2018). Morphological evolution and failure of LZC/YSZ DCL TBCs by electron beam-physical vapor deposition. Materialia *4*, 340–347.

Shen, Z.Y., He, L.M., Xu, Z.H., Mu, R.D., and Huang, G.H. (2019). LZC/YSZ DCL TBCs by EB-PVD: microstructure, low thermal conductivity and high thermal cycling life. J. Eur. Ceram. Soc. *39*, 1443–1450.

Shen, Z.Y., He, L.M., Mu, R.D., Xu, Z.H., and Huang, G.H. (2020). Effects of gradient transitional layer on thermal cycling life and failure of LaZrCeO/YSZ thermal barrier coatings. Corros. Sci. *163*, 108224.

Shen, Z.Y., Liu, G.X., Mu, R.D., He, L.M., Xu, Z.H., and Dai, J.W. (2021a). Effects of Er stabilization on thermal property and failure behavior of Gd$_2$Zr$_2$O$_7$ thermal barrier coatings. Corros. Sci. *185*, 109418.

Shen, Z.Y., Liu, Z., Mu, R.D., He, L.M., Liu, G.X., and Huang, Z.Y. (2021b). LaGdZrO/YSZ thermal barrier coatings by EB-PVD: microstructure, thermal properties and failure mechanism. Chem. Eng. J. Adv. *5*, 100073.

Shen, Z.Y., Liu, G.X., Mu, R.D., He, L.M., Xu, Z.H., and Dai, J.W. (2021c). Effects of Gd content on the phase structure and thermal property of (La$_{1-x}$Gd$_x$)$_2$(Zr$_{0.7}$Ce$_{0.3}$)$_2$O$_7$ ceramics. Open Ceram. *7*, 100144.

Shen, Z.Y., Liu, G.X., He, L.M., Mu, R.D., and Dai, J.W. (2022). Thermal property and failure behaviors of Gd doped LaZrCeO coatings with feathery microstructure. Npj Mater. Degrad. *6*, 17.

Song, D., Song, T., Paik, U., Lyu, G., Kim, J., Yang, S., and Jung, Y. (2020). Hot-corrosion resistance and phase stability of Yb$_2$O$_3$-Gd$_2$O$_3$-Y$_2$O$_3$ costabilized zirconia-based thermal barrier coatings against Na$_2$SO$_4$+V$_2$O$_5$ molten salts. Surf. Coat. Technol. *400*, 126.

Vaßen, R., Jarligo, M.O., Steinke, T., and Mack, D.E. (2010). Overview on advanced thermal barrier coatings. Surf. Coat. Technol. *205*, 938–942.

Wan, C.L., Qu, Z.X., Du, A., and Pan, W. (2009). Influence of B site substituent Ti on the structure and thermophysical properties of A$_2$B$_2$O$_7$-type pyrochlore Gd$_2$Zr$_2$O$_7$. Acta Mater. *57*, 4782–4789.

Wang, X.Z., Guo, L., Zhang, H.L., Gong, S.K., and Guo, H.B. (2015). Structural evolution and thermal conductivities of (Gd$_{1-x}$Yb$_x$)$_2$Zr$_2$O$_7$ (x=0, 0.02,

0.04, 0.06, 0.08, 0.1) ceramics for thermal barrier coatings. Ceram. Inter. *41*, 12621–12625.

Wu, F.S., Wu, P., Chen, L., and Feng, J. (2019). Structure and thermal properties of Al$_2$O$_3$-doped Gd$_3$TaO$_7$ as potential thermal barrier coating. J. Eur. Ceram. Soc. *39*, 2210–2214.

Yang, L.X., Zou, Z.H., Kou, Z.D., Chen, Y., Zhao, G.M., Zhao, X.F., Guo, F.W., and Xiao, P. (2017). High temperature stress and its influence on surface rumpling in NiCoCrAlY bond coat. Acta Mater. *139*, 122–137.

Zhang, X.F., Zhou, K.S., Deng, C.M., Liu, M., Deng, Z.Q., Deng, C.G., and Song, J.B. (2015). Gas-deposition mechanisms of 7YSZ coating based on plasma spray-physical vapor deposition. J. Eur. Ceram. Soc. *36*, 697–703.

Zhang, X.F., Deng, Z.Q., Li, H., Mao, J., Deng, C.M., Deng, C.G., Niu, S.P., Chen, W.L., Song, J.B., Fan, J.F., et al. (2020). Al$_2$O$_3$-modified PS-PVD 7YSZ thermal barrier coatings for advanced gas-turbine engines, npj Mater. Degrad *4*, 31.

Zhao, M., Pan, W., Wan, C.L., Qu, Z.X., Li, Z., and Yang, J. (2017). Defect engineering in development of low thermal conductivity materials: a review. J. Eur. Ceram. Soc. *37*, 1–13.

Zhou, X., He, L.M., Cao, X.Q., Xu, Z.H., Mu, R.D., Sun, J.B., Yuan, J.Y., and Zou, B.L. (2017). La$_2$(Zr$_{0.7}$Ce$_{0.3}$)$_2$O$_7$ thermal barrier coatings prepared by electron beam-physical vapor deposition that are resistant to high temperature attack by molten silicate. Corros. Sci. *115*, 143–151.

Zhou, X., Chen, T., Yuan, J.Y., Deng, Z.H., Zhang, H., Jiang, J.N., and Cao, X.Q. (2019). Failure of plasma sprayed nano-zirconia-based thermal barrier coatings exposed to molten CaO-MgO-Al$_2$O$_3$-SiO$_2$ deposits. J. Am. Ceram. Soc. *102*, 6357–6371.

Zhou, X., Song, W.J., Yuan, J.Y., Gong, Q.M., Zhang, H., Cao, X.Q., and Dingwell, D.B. (2020). Thermophysical properties and cyclic lifetime of plasma sprayed SrAl$_{12}$O$_{19}$ for thermal barrier coating applications. J. Am. Ceram. Soc. *103*, 5599–5611.

Zhou, X., Yan, S.L., Zhang, H., Dong, S.J., Li, X., Jiang, J.N., and Cao, X.Q. (2021). HVOF-sprayed AlSi50 alloy coatings as a novel electrothermal anti-icing/de-icing system for polymer-based composite structures. J. Therm. Spray Techn. *30*, 2161–2173.

STAR★METHODS

KEY RESOURCES TABLE

REAGENT or RESOURCE	SOURCE	IDENTIFIER
Chemicals		
ZrO_2	Sigma-Aldrich	CAS: 1314-23-4
Y_2O_3	Sigma-Aldrich	CAS: 1314-36-9
La_2O_3	Sigma-Aldrich	CAS: 1312-81-8
Sm_2O_3	Sigma-Aldrich	CAS: 12060-58-1

RESOURCE AVAILABILITY

Lead contact

Further information and requests for resources and reagents should be directed to and will be fulfilled by the Lead Contact, Zaoyu Shen (shenzaoyu@163.com).

Materials availability

This study did not generate new unique reagents.

Data and code availability

- All data reported in this work will be shared by the lead contact upon request.

- This work does not report original code and custom computer code.

- Any additional information required to reanalyze the data reported in this work paper is available from the Lead contact upon request.

EXPERIMENTAL MODEL AND SUBJECT DETAILS

This work does not use experimental models typical in the life sciences.

METHOD DETAILS

Preparation of TBCs

The substrate material was cut into 30.0 ×10 ×1.0 mm by wire cutting method. The NiCoCrAlYHf material was chosen for bond coating deposited by (AIP-PVD, A-1000 made by Russian). In the deposition process, the operating pressure was controlled below 5×10^{-2} Pa. The deposition rate of NiCoCrAlYHf is about 0.25 ± 0.5 μm/min. Then, the NiCoCrAlYHf bond coating was treated at 870°C for 3 h in vacuum heating process pressure (VBF-30 made by China). The thickness value of NiCoCrAlYHf bond coating is 30-40 μm. The composition of NiCoCrAlYHf bond coating is about 12.0 wt % Co, 20.0 wt % Cr, 10 wt % Al, 0.3 wt % Y, 0.2 wt % Hf and Ni as balance. LSZ ingots were synthesized by solid state reaction at 1500°C with La_2O_3 (99.99%), ZrO_2 (99.9%) and Sm_2O_3 (99.99%). The composition of LSZ ingots is about 45 at% La, 5 at% Sm, 50 at% Zr and O as balance. YSZ ingots were synthesized by solid state reaction at 1500°C with ZrO_2 (99.9%) and Y_2O_3 (99.99%). The YSZ and LSZ ingots were used in EB-PVD process (UE-207S, ICEBT). The specimen was heating to 850 ± 50°C with 20 ± 5 rpm. In the deposition process, the operating pressure was controlled below 1×10^{-2} Pa. The deposition rate of YSZ and LSZ coatings is about 3.5 ± 0.5 μm/min and 3.0 ± 0.5 μm/min, respectively. After the deposition of LaSmZrO coatings by EB-PVD, the atom ratio (La:Sm:Zr) of LaSmZrO coatings is about 1: 0.092:1.355.

Characterizations

The composition of coatings was measured by inductively coupled plasma-atomic emission spectrometry (ICP-AES; Agilent 725-ES). The crystal structure of coating was recorded by an X-ray powder diffractometer (XRD, Bruker D8 Advance). The morphology and composition of coating was further investigated by field emission scanning electron microscopy (FESEM, FEI Quanta 600) and transmission electron microscopy

CellPress
OPEN ACCESS

(TEM, EM-2100F). Element evolution was obtained by using an electron probe micro-analyzer (EPMA, JXA-8100 prototype). The thermal expansion coefficient of ceramics was detected by Netzsch DIL 402C from 200 to 1500°C. The thermal diffusivity (α) of ceramics was detected by Netzsch LFA 427.

Furnace cycle tests

Furnace cycle tests (thermal shock/cycling tests) of coatings were performed by a vertical furnace. The holding time of coatings was 55min/5min at 1100°C, and then the coatings were quenched by compressed air for 5 min to reduce the temperature below 300°C. In furnace cycle test, each coatings contains five parallel samples. The thermal durability of TBCs is the average number of 5 samples. The furnace cycle tests was finished until the broken area excess 10%.

QUANTIFICATION AND STATISTICAL ANALYSIS

Figures were analyzed by Origin from the raw data.

ADDITIONAL RESOURCES

This work does not include any additional resources.